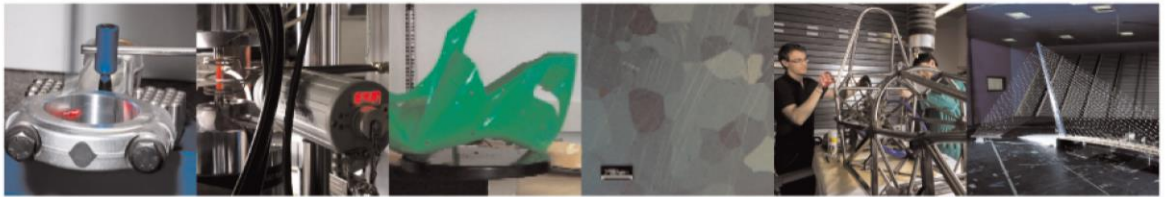




POLITECNICO  
MILANO 1863

DIPARTIMENTO DI MECCANICA



## Reduction of calibration effort in FEM-based optimization via numerical and experimental data fusion

COLOSIMO, BIANCA MARIA; PAGANI, LUCA; STRANO, MATTEO

This is a post-peer-review, pre-copyedit version of an article published in STRUCTURAL AND MULTIDISCIPLINARY OPTIMIZATION. The final authenticated version is available online at: <http://dx.doi.org/10.1007/s00158-014-1149-0>

This content is provided under [CC BY-NC-ND 4.0](https://creativecommons.org/licenses/by-nc-nd/4.0/) license



## Reduction of calibration effort in FEM-based optimization via numerical and experimental data fusion

Bianca Maria Colosimo · Luca Pagani · Matteo Strano

the date of receipt and acceptance should be inserted later

**Abstract** In this paper a fusion metamodeling approach is suggested as a method for reducing the experimental and computational effort generally required for calibrating the parameters of FEM simulations models. The metamodel is used inside an optimization routine for linking data coming from two different sources: simulations and experiments. The method is applied to a real problem: the optimal design of a metal foam filled tube to be used as an anti-intrusion bar in vehicles. The model is hierarchical, in the sense that one set of data (the experiments) is considered to be more reliable and it is labeled as “high-fidelity” and the other set (the simulations) is labeled as “low-fidelity”. In the proposed approach, Gaussian models are used to describe results of computer experiments because they are flexible and they can easily interpolate data coming from deterministic simulations. Since the results of experiments are obviously fully accurate, but aleatory, a second stage (“linkage”) model is used, which adjusts the prediction provided by the first model to more accurately represent the real experimental data. In the paper, the modeling and prediction ability of the method is first demonstrated and explained by means of artificially generated data and then applied to the optimization of foam filled tubular structures. The fusion metamodel yields comparable predictions (and optimal solution) if built over calibrated simulations vs. non-calibrated FEM models.

**Keywords:** Metamodeling, Metal Foams, Hierarchical Model, Stochastic Optimization, FEM, Calibration

---

Bianca Maria Colosimo  
Department of Mechanical Engineering, Politecnico di Milano E-mail: bianca-maria.colosimo@polimi.it

Luca Pagani  
Department of Mechanical Engineering, Politecnico di Milano E-mail: luca.pagani@polimi.it

Matteo Strano  
Department of Mechanical Engineering, Politecnico di Milano E-mail: matteo.strano@polimi.it

## 1 Introduction

The concept of metamodeling for computer simulations of manufacturing problems is known since more than two decades (Friedman and Pressman, 1988; Yu and Popplewell, 1994). At the beginning of this century, metal forming or plasticity numerical problems, which are usually very time consuming due to the complexity of physical phenomena involved at large deformations, have been increasingly metamodeled, for purposes like uncertainty assessment (Baghdasaryan et al, 2002) or design optimization (Do et al, 2004). The typical approach is to use a small set of experimental results in order to either tune or verify a Finite Element Method (FEM) model. Then, a metamodel can be built solely on the basis of accurate, calibrated, so-called “high-fidelity” simulations (Wiebenga et al, 2012). Alternatively, hierarchical metamodels have been proposed, based on a combination of “high-fidelity” (Hi-Fi) and “low-fidelity” (Lo-Fi) data sets (Kennedy and O’Hagan, 2000; Hino et al, 2006). In the available literature, high vs. low fidelity FEM models typically implies the use of finer vs. coarser meshes (Huang et al, 2006a). Alternatively, numerical models with different formulations have been used for modeling the same process: as an example in the optimization of sheet metal forming, outcome of a one-step solver (Lo-Fi) can be combined with data from an incremental solver (Hi-Fi) (Sun et al, 2010). Another example can be found in the field of CFD (Computational Fluid Dynamics), where a multistage metamodeling technique that links data coming from two different numerical sources (finite volumes and finite differences calculations) has been implemented (Qian et al, 2006). These “fusion” metamodels are used because they allow one to obtain accurate predictions with less computational effort than metamodels based only on Hi-Fi results, provided that Lo-Fi simulations are faster, thanks to a simpler formulation or to a coarser mesh. These models are often called hierarchical, because there is a hierarchy between different data sets. Clearly, the fidelity of numerical results can only be assessed with reference to real, experimental data of the physical process under investigation. In metal forming and plasticity problems, authors that deal with FEM simulations must spend a lot of time and effort in order to calibrate the most significant model parameters (coefficients of friction, flow stress and hardening parameters, anisotropy values, damage or failure thresholds, etc.) in order to match the numerical results. As an example, in (Roux and Bouchard, 2013), where a kriging metamodel is used for optimizing the strength of a clinched joint, an entire Section of the paper is devoted to the validation of the FEM model.

A different class of hierarchical models can be defined, that take into account the potential variability or uncertainty of the response, as in (Xia et al, 2011), where a hierarchical Bayesian model is implemented. These models have been more recently and therefore less frequently applied and they are suited not just for merging the results of Hi-Fi and Lo-Fi simulations, but for the fusion of computer experiments and physical experiments. The only available example of application in the metal forming industry, to the authors knowledge, is given in (Wagner et al, 2011), where the goal was to accurately model the temperature distribution of a work piece in a forging process. The results of experimental tests are inherently considered fully accurate, truly Hi-Fi, except for the only approximation due to the measurement system, but they are stochastic in nature and they are usually available in limited numbers, due to their high cost. The numerical results are considered Lo-Fi and deterministic.

In this paper a hierarchical, multi-stage metamodeling approach is proposed, similar to the one used in (Wagner et al, 2011), and combined to an optimization procedure. The goal of the present paper is to demonstrate that hierarchical metamodels can be used:

- not only to reduce to computational time spent in FEM calculations required for filling the design space, as in deterministic hierarchical models (Hino et al, 2006);
- not only to enrich the data base and yield a better overall model identification, as demonstrated in (Wagner et al, 2011);
- but also and especially to reduce the time and effort required for calibrating the FEM models.

In the proposed model, data coming from simulations are used to produce a first stage metamodel with a Kriging predictor based on a Gaussian process. Gaussian models are widely used to describe computer experiments data because they are flexible and they can easily interpolate points coming from nervous deterministic simulations. This metamodel can be very imprecise, because large deviations from real data can be expected in the simulations. Therefore, a second-stage model is used, in order to “correct” the prediction of the first model according to real experimental data observed. As for the first-stage model, a Gaussian process is used also to model this linkage or second-stage level. In this second-stage model a parameter can be added, known as the nugget, in order to take into account the process variability, i.e. the prediction does not interpolate the data and replicated measurements are allowed. The two-stages hierarchical model is then inserted in an optimization problem, which is solved using a version of EGO (Efficient Global Optimization) (Huang et al, 2006b; Roux and Bouchard, 2013). In the paper, the modeling and prediction ability of the method is first demonstrated and explained by means of artificially generated data. Then, the method is applied to a real problem: the optimal design of a metal foam filled tube to be used as an anti-intrusion bar.

## 2 The fusion metamodeling and the optimization approach

The problem we deal with consists of optimizing a response function, i.e. identifying the parameter setting that maximizes (or minimizes) the target response. Unfortunately, the objective function is not known in advance but it can be empirically observed via experimental data  $y_h(\mathbf{x})$ . The subscript  $h$  is added to denote Hi-Fi data, i.e., data that we trust because they are provided by real experiments on the phenomenon under interest. Due to process variability and measurement error, observed data are noisy and this is why optimization will concern the expected value of the empirical function.

Unfortunately, optimization via experimental modeling is a cumbersome activity, especially when the number of parameters is large and the experimental space to be spanned is wide. This is why an additional aid can be provided by numerical simulation data  $y_l(\mathbf{x})$ . Here, the subscript  $l$  stands for Lo-Fi data. As a matter of fact, numerical simulations are clearly a proxy of reality and optimization based on simulated data only can fail in identifying the real optimum. Furthermore, simulations usually require a calibration study at the beginning, in order to tune the

internal parameters of the simulator to achieve results which better resemble real data.

In this paper, we plan to show how appropriate modeling of the connection between real and simulation data, i.e., fusion metamodeling, allows one to: *i*) find the real optimum while reducing the overall experimental effort; *ii*) reducing (or even skipping) the initial calibration of the simulation, provided that the data fusion model can be interpreted as a way of performing off-line calibration.

Reduction of the overall effort is achieved by fusion metamodeling because this model provides a way to “transform” Lo-Fi data into Hi-Fi data. In other words, a model connecting the simulation and experimental results allows one to correct the simulation results ex-post, with respect to a given response variable of interest.

## 2.1 Fusion metamodeling

Suppose we have made a deterministic Lo-Fi simulation that depends on  $q$  parameters at  $n_l$  design points, where the sub-index  $l$  is used to denote the Lo-Fi data. A *first-stage* model can be built on these simulation results, by modeling the relationship between the response  $y_l$  and the design parameters. This function has usually a complex shape, so we use Gaussian Process (GP) model to describe its behavior. GPs, known as Kriging in spatial statistics, are widely used to describe response of a computer code (Santner et al, 2003). In particular, we assume that the response value  $y_l$  at a generic design point  $\mathbf{x}_i = (x_{i1}, x_{i2}, \dots, x_{iq})' \in \mathbb{R}^q$  can be described by the relation:

$$y_l(\mathbf{x}_i) = \mathbf{f}'_l(\mathbf{x}_i)\boldsymbol{\beta} + \eta(\mathbf{x}_i), \quad i = 1, \dots, n_l \quad (1)$$

where  $\mathbf{f}'_l(\mathbf{x}_i)$  is the transpose of  $\mathbf{f}_l(\mathbf{x}_i) \in \mathbb{R}^r$ , which is a vector of known basis functions (i.e., spline, Fourier, polynomial) which act as regressors,  $\boldsymbol{\beta} \in \mathbb{R}^r$  is a vector of unknown parameters,  $\eta(\mathbf{x}_i) \sim \mathcal{GP}(0, \sigma_\eta^2, \boldsymbol{\vartheta}_l)$  is a GP with zero mean and variance-covariance matrix defined through the parameter  $\sigma_\eta^2$  and the vector of scale parameters  $\boldsymbol{\vartheta}_l \in \mathbb{R}^q$ . The core of the GP is the variance-covariance matrix defined as:

$$\text{Cov}[\eta(\mathbf{x}_i), \eta(\mathbf{x}_j)] = \sigma_\eta^2 r_\eta(\mathbf{x}_i, \mathbf{x}_j) = \sigma_\eta^2 \exp\{-d(\mathbf{x}_i, \mathbf{x}_j)\}. \quad (2)$$

where  $r_\eta(\mathbf{x}_i, \mathbf{x}_j)$  is the correlation function modeling the dependence between two distinct design points  $\mathbf{x}_i$  and  $\mathbf{x}_j$  as a function of their distance. This type of correlation structure is useful when points that are close in the parameter space have similar responses and hence a good prediction at a given location can be done by looking at the responses observed in its neighborhood.

In this paper, the traditional power exponential function weight distance will be used, given by:

$$d(\mathbf{x}_i, \mathbf{x}_j) = \sum_{k=1}^q \vartheta_k^l |x_{ik} - x_{jk}|^{p_k}, \quad 0 < p_k \leq 2 \quad \forall k = 1, \dots, q \quad (3)$$

which allows one to model isotropy - i.e., similarity that does not depend on the specific direction in the design space - when all the scale parameters  $\vartheta_i^k$  in equation (3) assume the same value.

Let  $\mathbf{y}_l = (y_l(\mathbf{x}_1), y_l(\mathbf{x}_2), \dots, y_l(\mathbf{x}_{n_l}))'$  represent the response observed at the design points and  $\mathbf{F}_l = \begin{bmatrix} \mathbf{f}'_l(\mathbf{x}_1) \\ \mathbf{f}'_l(\mathbf{x}_2) \\ \vdots \\ \mathbf{f}'_l(\mathbf{x}_{n_l}) \end{bmatrix} \in \mathbb{R}^{n_l \times r}$  represent the matrix of regressors, estimation of all unknown GP parameters can be carried out by maximizing the logarithm of the restricted likelihood (Harville, 1977), given by:

$$l_{\hat{\beta}} = -\frac{n_l - r}{2} \log 2\pi + \frac{1}{2} \log (\mathbf{F}'_l \mathbf{F}_l) - \frac{n_l - r}{2} \hat{\sigma}_\eta^2 - \frac{1}{2} \log |\mathbf{R}_\eta| + \frac{1}{2} \log |\mathbf{F}'_l \mathbf{R}_\eta^{-1} \mathbf{F}_l| - \frac{n_l - r}{2} \quad (4)$$

where  $\mathbf{R}_\eta = \{r_\eta(\mathbf{x}_i, \mathbf{x}_j)\}$  is the correlation matrix,  $\hat{\sigma}_\eta^2 = \frac{1}{n_l - r} (\mathbf{y}_l - \mathbf{F}_l \hat{\beta})' \mathbf{R}_\eta^{-1} (\mathbf{y}_l - \mathbf{F}_l \hat{\beta})$  is the restricted maximum likelihood estimator of  $\sigma_\eta^2$  and  $\hat{\beta} = (\mathbf{F}'_l \mathbf{R}_\eta^{-1} \mathbf{F}_l)^{-1} \mathbf{F}'_l \mathbf{R}_\eta^{-1} \mathbf{y}_l$  is the maximum likelihood estimator of  $\beta$ . We used a *quasi-Newton* algorithm to optimize the function (4), using the Matlab `fmincon` function.

Once all the GP parameters have been estimated, prediction at any new design point  $\mathbf{x}_0$  can be computed using the BLUP (*Best Linear Unbiased Predictor*) estimator (see for example (Santner et al, 2003) or (Shabenberger and Gotway, 2005)), defined as:

$$\hat{y}_l(\mathbf{x}_0) = \mathbf{f}'_l(\mathbf{x}_0) \hat{\beta} + \hat{\mathbf{r}}'_\eta \hat{\mathbf{R}}_\eta^{-1} (\mathbf{y}_l - \mathbf{F}_l \hat{\beta}) \quad (5)$$

where  $\mathbf{r}_\eta = (r_\eta(\mathbf{x}_1, \mathbf{x}_0), r_\eta(\mathbf{x}_2, \mathbf{x}_0), \dots, r_\eta(\mathbf{x}_{n_l}, \mathbf{x}_0))'$  is the correlation vector between the new design point  $\mathbf{x}_0$  and all the other  $n_l$  points where the response was simulated.

Predictions obtained via equation (5) are based on the Lo-Fi simulations only. However, in most practical cases experimental results are available, too. We will refer to these results as  $y_h$  using the subscript  $h$  to denote the Hi-Fi data and distinguish them from the Lo-Fi ones. Usually,  $y_h$  are more accurate than  $y_l$  data but available in a limited number of locations, only (i.e.,  $n_h \ll n_l$ ).

The main objective of the fusion metamodeling is to combine the Lo-Fi and Hi-Fi data in order to improve predictions achievable by using the Lo-Fi or the Hi-Fi data sets alone. The core of the data fusion model is a *linkage* or *second-stage* model, which represents the connection between Lo-Fi and Hi-Fi data and can be expressed as (Kennedy and O'Hagan, 2000; Qian et al, 2006):

$$y_h(\mathbf{x}_i) = \rho(\mathbf{x}_i) \hat{y}_l(\mathbf{x}_i) + \delta_0 + \delta(\mathbf{x}_i) + \varepsilon_h(\mathbf{x}_i) \quad i = 1, \dots, n_h \quad (6)$$

where the aim is to correct the Lo-Fi predictions  $\hat{y}_l(\mathbf{x}_i)$  (i.e., predictions done using the Lo-Fi simulations only) using a "scale" and a "shift" effects, represented by  $\rho(\mathbf{x}_i)$  and  $\delta_0 + \delta(\mathbf{x}_i)$ , respectively. The term  $\varepsilon_h(\mathbf{x}_i)$  is the random term of the Hi-Fi points, known also as nugget, which is assumed to be independent and normally distributed, i.e.,  $\varepsilon_h(\mathbf{x}_i) \sim \mathcal{N}(0, \sigma_{\varepsilon_h}^2)$ . This nugget effect is included to represent randomness characterizing experimental data.

Following Qian et al (2006), the scale effect is assumed to have the expression

$$\rho(\mathbf{x}_i) = \mathbf{f}'_h(\mathbf{x}_i)\boldsymbol{\rho}, \quad (7)$$

where  $\mathbf{f}_h(\mathbf{x}_i)$  is a known basis function acting as the regressor term when computed at  $\mathbf{x}_i$  and  $\boldsymbol{\rho}$  is the vector of unknown parameters to be estimated. Subscript  $h$  is included to show that these regressors can be different from the ones assumed in equation (1). As a matter of fact, a first-order term (linear model) for  $\mathbf{f}_h(\mathbf{x}_i)$  is usually enough to model the scale effect (Qian et al (2006)).

The shift effect is represented by  $\delta_0 + \delta(\mathbf{x}_i)$ , where  $\delta_0$  is a constant and  $\delta(\mathbf{x}_i)$  is a GP:

$$\delta(\mathbf{x}_i) \sim \mathcal{GP}(0, \sigma_\delta^2, \boldsymbol{\vartheta}_h). \quad (8)$$

As in the Lo-Fi model, we will use the power exponential correlation function to describe the correlation structure of the shift effect. It is possible to prove (Pagani, 2011) that only  $\delta_0$  can be computed in closed form as:

$$\hat{\delta}_0 = \frac{\mathbf{1}'_{n_h} \boldsymbol{\Sigma}_h^{-1} (\mathbf{y}_h - \mathbf{P} \hat{\mathbf{y}}_l)}{\mathbf{1}'_{n_h} \boldsymbol{\Sigma}_h^{-1} \mathbf{1}_{n_h}}, \quad (9)$$

where  $\mathbf{y}_h = (y_h(\mathbf{x}_1), y_h(\mathbf{x}_2), \dots, y_h(\mathbf{x}_{n_h}))'$  are the observed Hi-Fi data,  $\mathbf{P}$  is a diagonal matrix with entries  $\rho(\mathbf{x}_i)$  (shown in equation (7)) for  $i = 1, \dots, n_h$  and  $\boldsymbol{\Sigma}_h$  is known as the mean square prediction error (MSPE) or kriging variance. The kriging variance can be computed as  $\boldsymbol{\Sigma}_h = \mathbf{P} \boldsymbol{\Sigma}_0 \mathbf{P}' + \sigma_\delta^2 \mathbf{R}_\delta + \sigma_{\varepsilon_h}^2 \mathbf{I}_{n_h}$ , where  $\boldsymbol{\Sigma}_0$  is the kriging variance of the Low-Fi model shown in equation (2), computed at locations where Hi-Fi data have been observed,  $\mathbf{R}_\delta = \{r_\delta(\mathbf{x}_i, \mathbf{x}_j)\}$  is the correlation matrix of the GP assumed in equation (8) for the shift effect  $\delta(\mathbf{x}_i)$ ,  $\mathbf{I}_{n_h} \in \mathbb{R}^{n_h \times n_h}$  is an identity matrix and  $\mathbf{1}_{n_h} \in \mathbb{R}^{n_h}$  is a vector of ones. Also in this case, the other unknown parameters can be found by maximizing the logarithm of the restricted likelihood (Harville, 1977) given by:

$$l_{\hat{\delta}_0} = -\frac{n_h}{2} \log 2\pi + \frac{1}{2} \log |\mathbf{F}'_h \mathbf{F}_h| - \frac{1}{2} \log |\boldsymbol{\Sigma}_h| - \frac{1}{2} \log |\mathbf{F}'_h \boldsymbol{\Sigma}_h^{-1} \mathbf{F}_h| + \quad (10)$$

$$-\frac{1}{2} \left( \mathbf{y}_h - \mathbf{P} \hat{\mathbf{y}}_l - \hat{\delta}_0 \mathbf{1}_{n_h} \right)' \boldsymbol{\Sigma}_h^{-1} \left( \mathbf{y}_h - \mathbf{P} \hat{\mathbf{y}}_l - \hat{\delta}_0 \mathbf{1}_{n_h} \right).$$

where  $\mathbf{F}_h = \begin{bmatrix} \mathbf{f}'_h(\mathbf{x}_1) \\ \mathbf{f}'_h(\mathbf{x}_2) \\ \vdots \\ \mathbf{f}'_h(\mathbf{x}_{n_h}) \end{bmatrix} \in \mathbb{R}^{n_h \times s}$ .

According to the assumed combination of the linkage (or “second-stage”) (6) and “first-stage” (1) models, the metamodel obtained via data fusion allows one to predict a process realization at each new location  $\mathbf{x}_0$  as:

$$\hat{y}_h(\mathbf{x}_0) = \hat{\rho}(\mathbf{x}_0) \hat{y}_l(\mathbf{x}_0) + \hat{\delta}_0 + \left( \hat{\sigma}_\delta^2 \mathbf{r}_\delta + \hat{\sigma}_0 \right)' \hat{\boldsymbol{\Sigma}}_h^{-1} \left( \mathbf{y}_h - \hat{\mathbf{P}} \hat{\mathbf{y}}_l - \hat{\delta}_0 \mathbf{1}_{n_h} \right) \quad (11)$$

where  $\mathbf{r}_\delta = \text{Corr}(\mathbf{y}_h, y_h(\mathbf{x}_0))$ ,  $\boldsymbol{\sigma}_0$  is a vector with entries  $\sigma_{0i} = \rho(\mathbf{x}_i) \cdot \rho(\mathbf{x}_0) \cdot \text{Cov}(\hat{y}_l(\mathbf{x}_i), \hat{y}_l(\mathbf{x}_0)) \forall i = 1, \dots, n_l$ .

It is worth noting that this linkage model can be interpreted as an off-line calibration step, where the Lo-Fi data are transformed to Hi-Fi data, depending

on the specific locations where the points are observed. This effect will be further explored as a possible way to reduce or even skip the traditional pre-tuning of the simulation model, where internal parameters of the simulation model are tuned to make simulation resemble experimental data.

## 2.2 Example of metamodeling performance with artificially generated data

In order to show effectiveness of the proposed metamodel, this section shows an example of metamodeling starting from artificially generated data. We will compare four different metamodels: a model based on the Lo-Fi points only (LF), a model based on the Hi-Fi points (HF) only, and two models based on combining Lo-Fi and Hi-Fi points. In particular, in the third approach that will be referred to as additive (ADD), the two data sets are simply merged and considered as they come from a common source. In the fourth case, referred to as fusion (F), the two datasets are merged with the proposed metamodeling approach.

In the following, we will use the letter  $z_{\bullet}$  to represent the real model from which we will draw samples and is not known in real practice. We will keep the previous notation and use the letter  $y_{\bullet}$  to represent all the models estimated from the observed data according to our metamodeling approaches.

In this example, the true response  $z$ , depends on two variables,  $x_1$  and  $x_2$ , i.e.,  $q = 2$ . Without loss of generality, we consider two variables only, to better visualize the reconstruction in a surface plot.

We assume that the real surface is described by:

$$z(x_1, x_2) = (1 - x_1)^2 e^{-x_1^2 - (x_2 + 1)^2} - 10 \left( \frac{x_1}{5} - x_1^3 - x_2^5 \right) e^{-x_1^2 - x_2^2} + \frac{1}{3} e^{-(x_1 + 1)^2 - x_2^2} \quad (12)$$

and the Hi-Fi data are given by:

$$z_h(x_1, x_2) = z(x_1, x_2) + \varepsilon_h, \quad (13)$$

where  $\varepsilon_h \sim \mathcal{N}(0, \sigma_h^2)$ . In other words, the experimental data are noisy observations of the real surface.

In our example, the Lo-Fi response is given by:

$$z_l(x_1, x_2) = z(x_1, x_2) + a (x_1^2 + x_2^2), \quad (14)$$

where  $a$  is a constant that control the systematic error given by the term  $(x_1^2 + x_2^2)$ , whose pattern is shown in Figure 1(a) (assuming  $a = 0.3$ ). The Lo-Fi response has no random term because we assumed deterministic simulations.

In Figure 1(b) the “real” surface (i.e. in equation (12)) is shown together with 20 data drawn from the Hi-Fi model in equation (13) and 200 data from the Lo-Fi model in equation (14). In the following, all the data are drawn according to the *maxmin* latin hypercube criterion, which is widely used in computer experiments (Santner et al, 2003).

In order to graphically compare the predicting ability of the four models, Figure 2(a) shows a cross section of the reconstructed and real surfaces at  $x_1$  equal to 0.04, while  $x_2$  is varying on the abscissa. When prediction is done using the LF

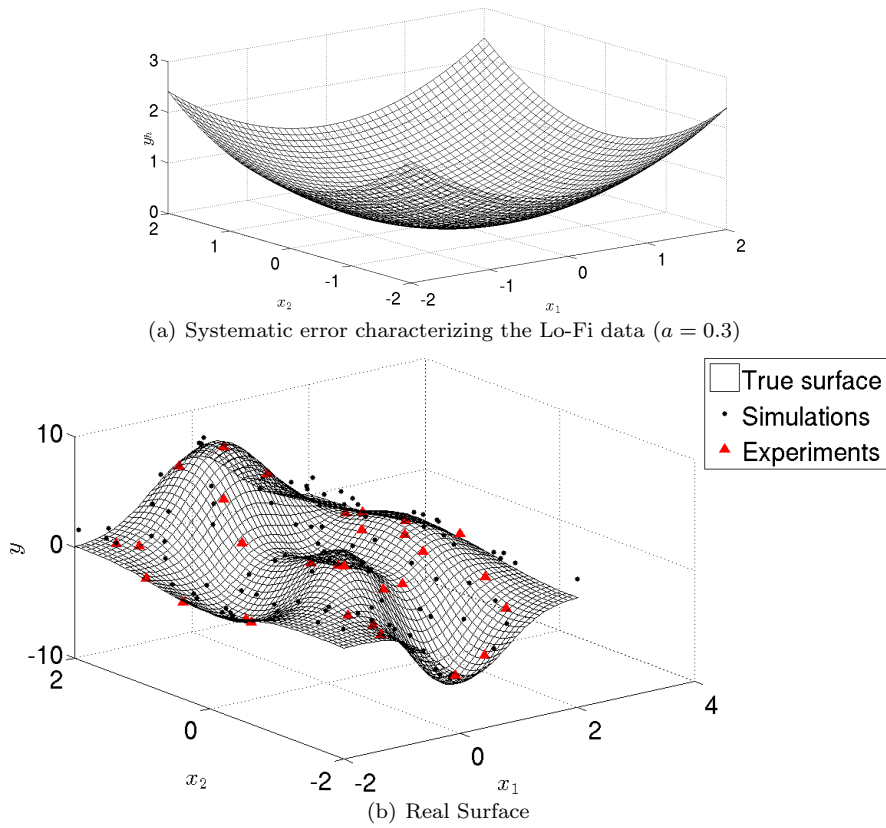
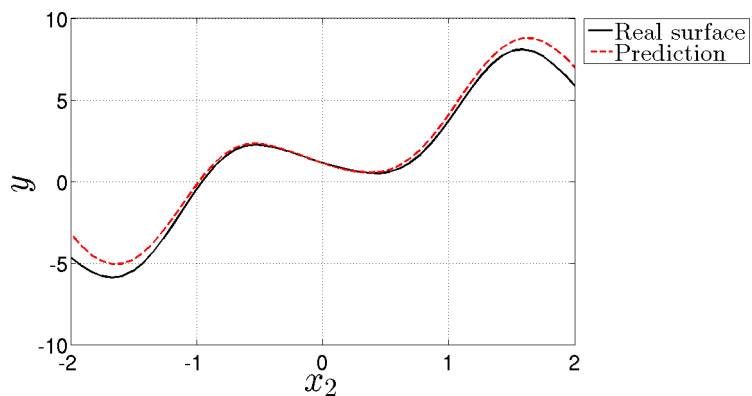
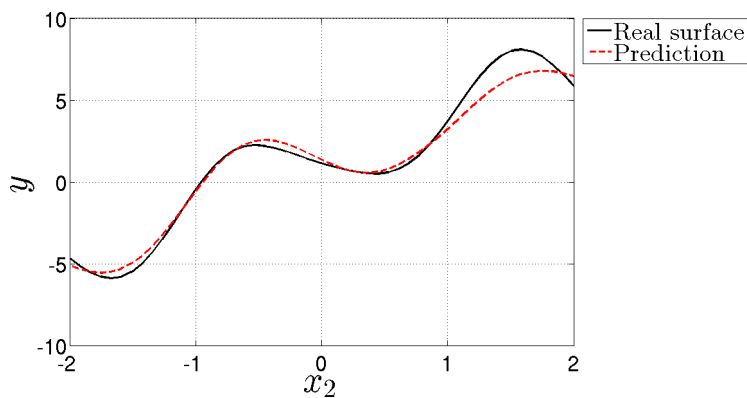


**Fig. 1** Systematic error characterizing the Lo-Fi data and real surface to be reconstructed together with simulated data points.

model (i.e., prediction based on a GP model based on 200 Lo-Fi data only) a significant reconstruction error is clear at the borders, due to the systematic error characterizing Lo-Fi data. In case of the HF model (where reconstruction is based on 20 Hi-Fi data only), the reconstruction error is wide in region where not enough data are available (Figure 2(b)). The ADD model obtained by performing GP fitting on all the 220 Lo-Fi plus Hi-Fi data (Figure 3(a)) shows a pattern similar to the one observed for the LF model, with little prediction improvement. This is due to the fact that the response surface is ruled by the large number of Lo-Fi data points (and by their systematic error), since they are ten times the number of Hi-Fi points. Finally, the fusion model F is shown in (Figure 3(b)). In this case the reconstruction is similar to the one observed for the LF model, but thanks to the hierarchical distinction between the Hi-Fi and Lo-Fi data, it is very close to the real surface.

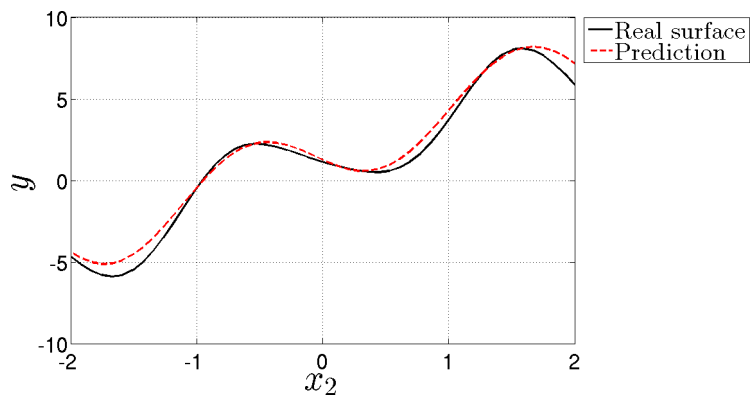


(a) Low-Fidelity model - LF

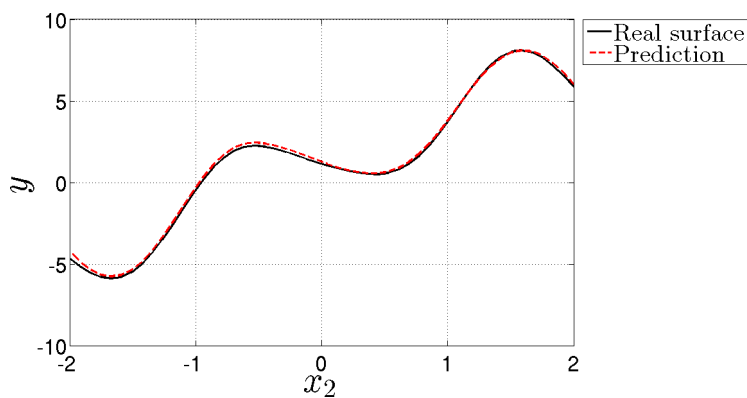


(b) High-Fidelity model - HF

**Fig. 2** Cross sections of the surface reconstruction for the LF and HF models at  $x_1 = 0.04$



(a) Addition model - ADD



(b) Fusion model - F

**Fig. 3** Cross sections of the surface reconstruction for the A and F models at  $x_1 = 0.04$

All the qualitative conclusions drawn from Figure 3 can be confirmed using the mean square prediction error (MSE) as performance indicator. The MSE computes the mean value of the reconstruction error and is computed as follows:

$$\text{MSE} = \frac{\sum_{i=1}^n (z_i - \hat{y}_i)^2}{n} \quad (15)$$

where  $z_i$  is the actual value of the function and  $\hat{y}_i$  is the value predicted at the same location considering one of the four competitive models (HF, LF, A, F). Figure 4 shows the 95% confidence interval of the MSE based on 10 replicates of the reconstruction process ( $a = 0.3$  and  $\sigma_h^2 = 0.1$ ). In each replication, a latin hypercube sampling was performed to select the points' locations, in order to check the prediction ability of each model, while taking into account also this source of variability. The confidence intervals of all the models are shown in Figure 4(a). A different scale has been used in Figure 4(b) in order to better clarify the differences among the LF, ADD and F models. Clearly, the F model outperforms all the other three models.

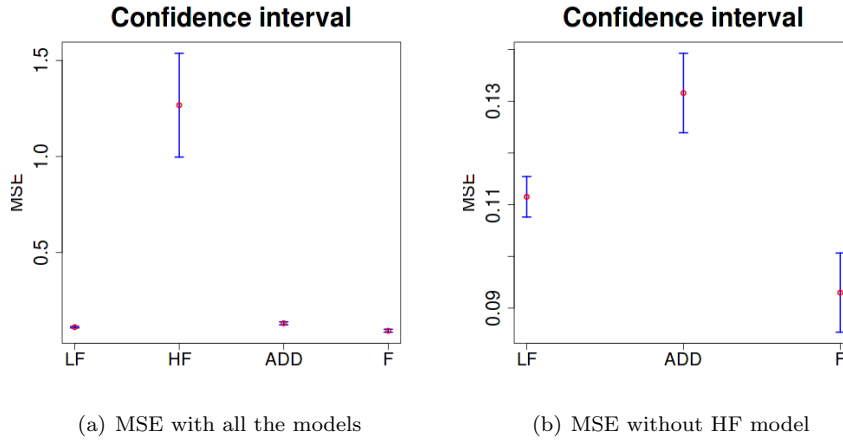
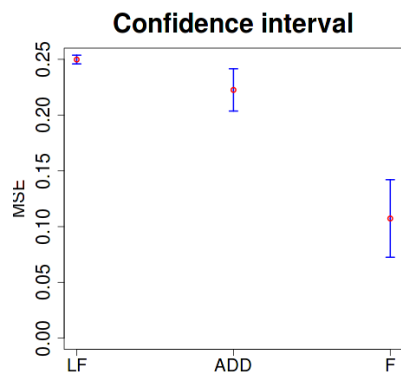


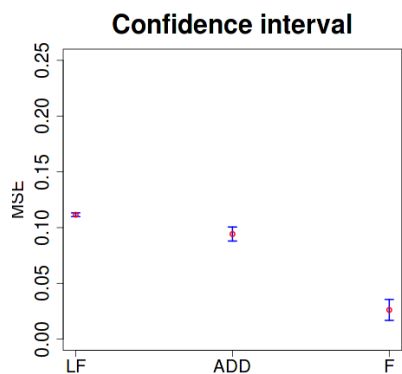
**Fig. 4** Performance comparison among the four metamodels

A sensitivity analysis was eventually carried out in order to check whether advantages of the proposed model still hold when different scenarios are considered. We repeated the previous comparison by changing the systematic error  $a$  (from 0.3 to 0.2) and the random noise variance  $\sigma_h^2$  (from 0.1 to 0.5). All the  $2^2 = 4$  combinations of the changing parameters were considered. One of these scenarios ( $a = 0.3$  and  $\sigma_h^2 = 0.1$ ) was already explored as reference test case (Figure 4), and hence Figure 5(a) shows results of the remaining three scenarios. As for the previous case, the HF model has poor performance and has a very large confidence interval, this is why it is not shown in the plots. As is clear from the first picture, increasing the  $\sigma_h^2$  to 0.5, i.e. considering a higher variability of the Hi-Fi data, results in an increased variability of the MSE for the F model but without changing its superiority. The effect of decreasing the systematic error (i.e.,  $a$  set equal to 0.2), is shown in Figure 5(b). Both the LF and the ADD model increase their

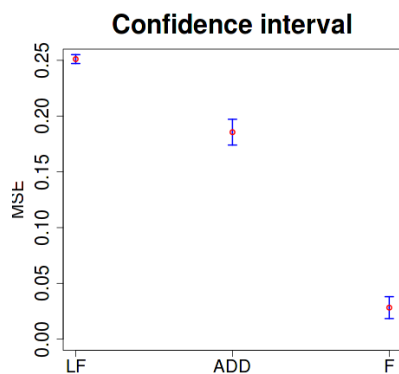
prediction performance, but the F model is still the best one. Finally, if we increase the random noise up to 0.5 and decrease the systematic error coefficient down to 0.2, the comparison of the MSE is shown in Figure 5(c). In this case, the LF model is better than the ADD model because of the high random noise, but the F model is again the best.



(a)  $a = 0.3, \sigma_h^2 = 0.5$



(b)  $a = 0.2, \sigma_h^2 = 0.1$



(c)  $a = 0.2, \sigma_h^2 = 0.5$

**Fig. 5** Performance comparison changing parameters

### 2.3 The optimization approach

The final goal of the paper is to show how an appropriate data fusion based on combining simulated and experimental data can result in an efficient optimization procedure, which can significantly reduce the simulation and calibration efforts.

In this case, optimization consists of finding the design point  $\mathbf{x}$  such that the expected value of the response function is maximized (or minimized). In our case, the expected value of the response function is computed via equation (11), which shows prediction of the response function in any location using the metamodel built on data fusion. In the following, without loss of generality, we assume that the response function has a unique global maximum.

Optimization based on a kriging metamodel is usually performed with the *Efficient Global Optimization* (EGO) algorithm, originally proposed by Jones et al (1998). The EGO algorithm looks for the global minimum of a generic deterministic function, using GP for computing predictions at any new location. The algorithm was extended in order to take into account also noisy functions in (Huang et al, 2006b) and in (Huang et al, 2006a).

The first step of the optimization algorithm consists of finding an initial guess of the response surface, by selecting an initial number of  $10q$  points to roughly estimate the underlying surface, where  $q$  is the dimension of the function domain. After a first rough estimation of the function, the algorithm suggests adding a point where a criterion, called the Expected Improvement (EI) (Mockus et al, 1978), is maximized. Then, the algorithm is re-iterated until a stopping criterion is satisfied (usually when the ratio between the EI at the  $j$ -th step and the initial EI becomes  $10^{-2}$ ).

In our paper, a deterministic model (i.e., model without random term) is used to describe the simulation results. It is combined with a model including a nugget effect (random term) when simulated data are linked to experimental results. We will assume that the new points added in the optimization procedure to achieve the optimum are simulated and hence not affected by noise. This is why the classical EI criterion (not the augmented EI function proposed in (Huang et al, 2006b) to deal with noisy data) will be used. However, following our metamodel strategy, any new Lo-Fi simulation will be “translated” into the corresponding Hi-Fi data, thanks to the linkage model developed in the data fusion procedure (equation 11).

In the following, the details of the EGO algorithm in the version suitable to optimize our two-stage metamodel will be described. At each iteration, the current maximum is established as the maximum of the values predicted via the fusion metamodel (i.e., the model combining both simulations and experimental data) in all the locations where simulations or real data were observed. Let  $\hat{y}_{l,max}$  represent this current maximum, i.e.  $\max_i \hat{y}_l$ .

A new variable  $Q(\mathbf{x})$  is defined as the difference between the metamodel  $\hat{y}_h(\mathbf{x})$  predicted at a generic location  $\mathbf{x}$  and the current maximum:

$$Q(\mathbf{x}) = \hat{y}_h(\mathbf{x}) - \hat{y}_{l,max} \sim \mathcal{N}(\mu_Q(\mathbf{x}), \sigma_Q^2(\mathbf{x})) \quad (16)$$

The expected improvement can be thus written as a function of this new variable  $Q$ , representing the difference between the objective function and the current optimum, namely:

$$\begin{aligned} \text{EI}(\mathbf{x}) &= \mathbb{E}(\max\{Q(\mathbf{x}), 0\}) = \int_0^{+\infty} \frac{q}{\sqrt{2\pi\sigma_Q^2(\mathbf{x})}} e^{-\frac{1}{2} \frac{(q-\mu_Q(\mathbf{x}))^2}{\sigma_Q^2(\mathbf{x})}} dq \\ &= \sigma_Q(\mathbf{x}) \varphi\left(\frac{\mu_Q(\mathbf{x})}{\sigma_Q(\mathbf{x})}\right) + \mu_Q(\mathbf{x}) \Phi\left(\frac{\mu_Q(\mathbf{x})}{\sigma_Q(\mathbf{x})}\right). \end{aligned} \quad (17)$$

The main task is now finding the input combination  $\mathbf{x}$  that maximizes EI and this requires one to be able to compute the distribution of  $Q$  at any location  $\mathbf{x}$ . To this aim, we consider a new location  $\mathbf{x}_0$  and we build a bi-variate vector consisting of the metamodel prediction at this new location  $\hat{y}_h(\mathbf{x}_0)$  and the current maximum  $\hat{y}_{l,max}$ . It is possible to prove (see (Pagani, 2011)) that this vector is approximately distributed as a bi-variate normal:

$$\begin{bmatrix} \hat{y}_h(\mathbf{x}_0) \\ \hat{y}_{l,max} \end{bmatrix} \approx \mathcal{N}_2(\boldsymbol{\mu}_{ego}, \boldsymbol{\Sigma}_{ego}) \quad (18)$$

with

$$\begin{aligned} \boldsymbol{\mu}_{ego} &= \mathbf{P}_{\mathbf{X}_0} \hat{\mathbf{y}}_l(\mathbf{X}_0) + \hat{\delta}_0 \mathbf{1}_2 + \left( \hat{\sigma}_\eta^2 \hat{\mathbf{R}}_{\delta_{\mathbf{X}_h, \mathbf{X}_0}} + \hat{\boldsymbol{\Sigma}}_{l_{\mathbf{X}_h, \mathbf{X}_0}} \right)' \hat{\boldsymbol{\Sigma}}_h^{-1} \left( \mathbf{y}_h - \hat{\mathbf{P}} \hat{\mathbf{y}}_l - \hat{\delta}_0 \mathbf{1}_{n_h} \right) \\ \boldsymbol{\Sigma}_{ego} &= \hat{\boldsymbol{\Sigma}}_{h_{\mathbf{X}_0}} - \hat{\boldsymbol{\Sigma}}'_{h_{\mathbf{X}_h, \mathbf{X}_0}} \hat{\boldsymbol{\Sigma}}_h^{-1} \hat{\boldsymbol{\Sigma}}_{h_{\mathbf{X}_h, \mathbf{X}_0}} + \\ &\quad + \frac{\left( \mathbf{1}_2 - \hat{\boldsymbol{\Sigma}}'_{h_{\mathbf{X}_h, \mathbf{X}_0}} \hat{\boldsymbol{\Sigma}}_h^{-1} \mathbf{1}_{n_h} \right) \left( \mathbf{1}_2 - \hat{\boldsymbol{\Sigma}}'_{h_{\mathbf{X}_h, \mathbf{X}_0}} \hat{\boldsymbol{\Sigma}}_h^{-1} \mathbf{1}_{n_h} \right)'}{\mathbf{1}'_{n_h} \hat{\boldsymbol{\Sigma}}_h^{-1} \mathbf{1}_{n_h}} \end{aligned}$$

where  $\mathbf{X}'_0 = [\mathbf{x}_0, \mathbf{x}_{max}]$ ,  $\mathbf{X}'_h = [\mathbf{x}_1, \mathbf{x}_2, \dots, \mathbf{x}_{n_h}]$  is the matrix of Hi-Fi points,  $\mathbf{R}_{\delta_{\mathbf{X}_h, \mathbf{X}_0}}$  is the correlation matrix between  $\mathbf{X}_h$  and  $\mathbf{X}_0$ ,  $\boldsymbol{\Sigma}_{l_{\mathbf{X}_h, \mathbf{X}_0}}$  is the covariance matrix between  $\rho(\mathbf{X}_h) \hat{\mathbf{y}}_l(\mathbf{X}_h)$  and  $\rho(\mathbf{X}_0) \hat{\mathbf{y}}_l(\mathbf{X}_0)$ ,  $\boldsymbol{\Sigma}_{h_{\mathbf{X}_0}}$  is the covariance matrix of  $\mathbf{X}_0$  and  $\boldsymbol{\Sigma}_{h_{\mathbf{X}_h, \mathbf{X}_0}}$  is the covariance matrix between  $\mathbf{X}_h$  and  $\mathbf{X}_0$ . Clearly, the distribution of  $Q(\mathbf{x})$  can be now computed starting from the aforementioned bi-variate vector, by applying standard multivariate statistical theory:

$$Q(\mathbf{x}) \approx \mathcal{N}(c' \boldsymbol{\mu}_{ego}, c' \boldsymbol{\Sigma}_{ego} c) \quad (19)$$

where  $c = (1, -1)'$ .

Now that the distribution of  $Q$  in equation 17, can be computed, optimization of the function can be carried out (using for instance a Matlab global optimization algorithm based on (Zsolt et al, 2007)).

We note that the EGO algorithm requires a new estimation of  $\hat{y}_h(\mathbf{x})$ ,  $\hat{y}_{l,max}$  and  $\mu_Q(\mathbf{x})$  and  $\sigma_Q(\mathbf{x})$  at each step.

#### 2.4 Example of optimization performance with artificially generated data

In this section we will show how the EGO procedure works, with reference to the example described in section 2.2 (with  $a$  equal to 0.3 and  $\sigma_h^2$  equal to 0.5). An initial design of 20 Lo-Fi points and 10 Hi-Fi points, selected according to a *maximin* latin hypercube will be considered.

Figure 6 shows the surface predicted before (6(a)) and after (6(b)) the EGO algorithm. As clear from the plot, the EGO algorithm concentrates simulations in the neighborhood of the maximum value, thus allowing for a better estimation of the true surface in that region.

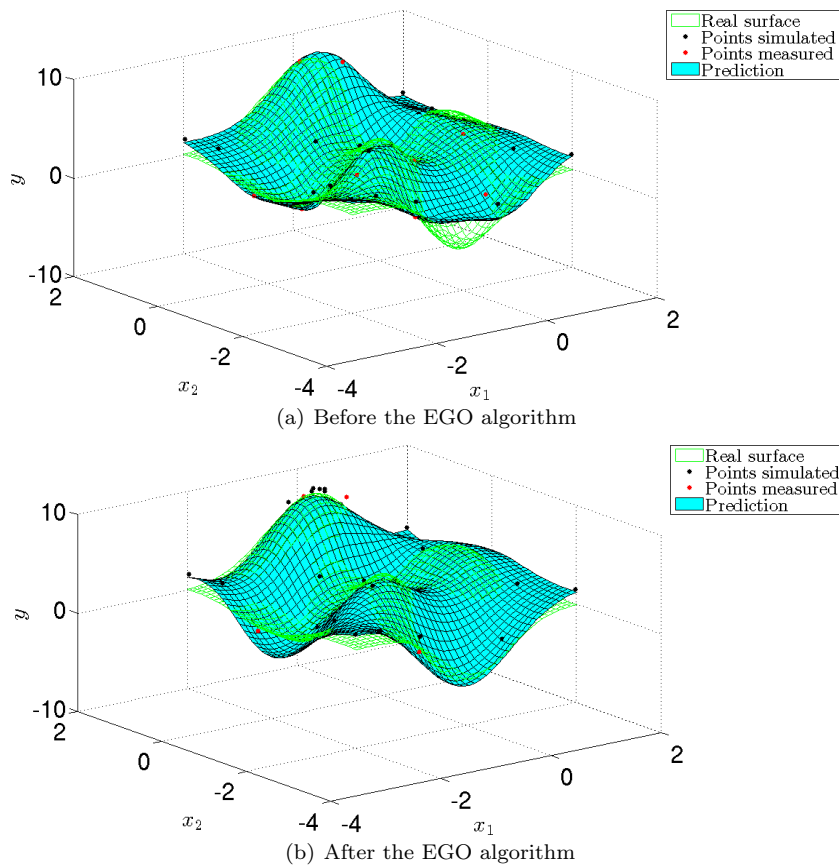


**Fig. 6** Surface estimation before and after the EGO algorithm

In order to test the ability of the EGO approach to converge, the optimization based on our two-stages metamodel was repeated 10 times, starting from different starting points at each run. Table 1 summarizes results of these simulations, showing the number of iterations required before convergence together with the difference between the true values of the maximum coordinates (i.e.,  $x_1$ ,  $x_2$  and  $y$ , respectively) and the values of the optimum found by our proposed method. As clear from the table, the error is consistently low, if compared to the range of the 3 variables.

# iterations before convergence	difference with true optimal $x_1$	difference with true optimal $x_2$	difference with true optimal $y$
4	-0.0424	-0.0124	0.0088
11	0.0429	0.0040	-0.0154
6	-0.0549	-0.0124	-0.0075
5	-0.0429	-0.0092	0.0107
6	0.0427	-0.0110	-0.0097
6	0.0088	0.0135	0.0064
4	-0.0416	-0.0098	-0.0104
5	-0.0404	-0.0137	0.0078
6	-0.0415	0.0125	-0.0086
6	0.0394	-0.0167	-0.0055

**Table 1** Number of iterations of ten replicates required by the EGO algorithm and difference of the optimum coordinates found with respect to the coordinates of the true maximum value

Statistical tests to check the equality between the coordinates of the true maximum and the coordinates of the EGO solutions were eventually performed. The p-values of the tests were 0.69, 0.66 and 0.97, respectively for  $x_1$ ,  $x_2$  and  $y$ . Therefore, there was no statistical evidence to indicate that the real solution and the one found by the EGO approach are different.

### 3 Optimization via data fusion and the calibration advantage: the real case study

The modeling and optimization procedure described in Section 2 will be applied to a real optimization problem: the design of an anti-intrusion side bar for vehicles, made of an outer tubular steel case and a filling reinforcement made of aluminum foam (Strano et al, 2010). The filling of cases made of thin metal sheets or tubes with a reinforcement made of cellular metals (or metal foams), as for the structure shown in Figure 7, allows for the production of lightweight, high performance components, particularly suited for flexural resistance in terms of amount of energy absorbed for a given maximum load.



**Fig. 7** Steel tube

In order to optimize the performance of the component in case of an accident, several issues must be taken into account. Let us consider a closed section with a composite (bi-material) structural beam with initial length  $L$ , vertical average dimension  $H$ , horizontal average size  $W$ , initial average cross section area  $S = H \cdot W$ , total occupied volume  $V = S \cdot L$ , mass  $M$ , apparent density  $\rho = \frac{V}{M}$ . In lateral

impact, the structure will undergo a flexural state of stress-strain. Given a load  $P$  [ $kN$ ] - deflection  $\delta l$  [ $mm$ ] diagram in bending of a foam filled bar, up to any value of deflection  $\delta l$ , the load curve profile will exhibit a maximum load value  $P_{max}$ , an average load  $P_{avg}$  and an amount of absorbed energy per volume  $E_{abs} = P_{avg} \cdot \delta l$ . The crash force efficiency can be written as the ratio between the mean load and the maximum load of a Force-Displacement curve (Yuen and Nurick, 2008):  $\eta = \frac{P_{avg}}{P_{max}}$ . A body with high efficiency will have a large energy absorption, while limiting the maximum load  $P_{max}$  (and the corresponding acceleration) transmitted to the vehicle. A Specific Energy Absorption ( $SEA$ ) can be also defined, as the ratio between the absorbed energy and the total mass:  $SEA = \frac{E_{abs}}{M}$ . In a lateral crash, for any given tubular composite structure and a given amount of incoming energy, it is important to achieve the competing objectives listed as follows.

- To increase or maximize the energy absorption  $E_{abs}$ , given a maximum deflection  $\delta l_{max}$ , while limiting the total mass  $M$ ; this is equal to maximizing the  $SEA$  of the structure.
- To increase or maximize the crash force efficiency  $\eta$ .
- To minimize the intrusion into the vehicle  $\delta l_{max}$ .

Let  $\mathbf{x}$  represent a design variable influencing the aforementioned indicators, a synthetic objective function  $y$  can be built as follows:

$$y(\delta l_{max}, \mathbf{x}) = \frac{SEA(\delta l_{max}, \mathbf{x}) \cdot \eta(\delta l_{max}, \mathbf{x})}{\delta l_{max}} = \frac{P_{avg}^2(\delta l_{max}, \mathbf{x})}{P_{max}(\delta l_{max}, \mathbf{x}) \cdot M(\mathbf{x})} \quad (20)$$

and measured in [ $\frac{kN}{kg}$ ]. In the present case, the maximum admissible intrusion was set to  $\delta l_{max} = 48$   $mm$  for reasons related to design criteria of cars. In the previous expression, a design vector  $\mathbf{x}$  is introduced. This vector represents the design variables, which are known to influence the response even if the analytical expression modeling this influence is not known in advance. This is a typical problem in engineering design, where simulations and/or experimental data are required to empirically reconstruct the relationship between the design variables and the response function thus allowing optimization. In our case, our design vector is made of two design variables. The first  $x_1$  is a toughness indicator, related to the plastic material properties of the outer steel skin. The second variable  $x_2$  is a shape factor, related to its geometry.

$$x_1 = \frac{n^{n+1} \cdot K}{n + 1} \quad (21)$$

$$x_2 = \frac{J}{W} \quad (22)$$

where  $K$  and  $n$  are respectively the hardening coefficient and exponent of the flow stress power law,  $J$  is the moment of inertia of the tube cross section and  $W$  is the depth of the specimen, in the direction of the movement of the punch, i.e. the lateral encumbrance of the structure.  $x_1$  [ $MPa$ ] measures the fracture toughness of the skin material, because it represents the area under the flow stress curve. In  $x_2$  [ $mm^3$ ],  $J$  is divided by  $W$  because it is important to keep the encumbrance under control, due to the limited space available inside the car door.

Both the design variables affect the response function  $y$ . Unfortunately, the way in which these two design variables affect the response is not analytically known and has to be detected via simulation and/or experimental data.

The optimization problem can be formalized as finding the  $\boldsymbol{x}$ -value that maximizes  $y$ , within the range of the investigated values of  $\boldsymbol{x}$ . Simulations of the three-point bending tests were run with an FEM model with explicit time integration scheme. The foam was modeled with 3D hexahedral elements with a ‘‘Crushable Foam’’ isotropic material formulation. The tube was modeled with shell elements with an elastic-plastic isotropic material formulation. Contact between foam and tube was modeled with a penalty formulation and a Coulomb coefficient of friction equal to 0.6. The number of elements changed according to the simulated structure and the simulation time for each test ranges between 4 and 8 CPU hours. Each simulation was therefore quite expensive from a computational viewpoint. This is a typical situation in optimization problems where large plastic deformations are involved, due to the strong nonlinearities of the computational problem. Each experimental test was also both time- and money-consuming because of the manufacturing process of foam filled tube, which is described in (Strano et al, 2010). Since both simulations and experiments were expensive, any mathematical technique aimed at reducing the number of design points required for optimization would be highly appreciated in the field of design and manufacturing optimization of metal foam based structures. The common approach used in the scientific literature in this case is generally based on the following steps:

1. running a limited number of experiments,
2. building the numerical model and iterating until a satisfactory calibration of the simulation model is reached,
3. running the simulations required for metamodeling and optimization.

Calibration is often not described in scientific papers, and the final calibrated model is generally presented, as in (Zarei and Kroger, 2008). Nevertheless, step 2 is always required, although not explicitly mentioned. The aim of this paper is to demonstrate how the fusion metamodel can be used for merging steps 2 and 3, reducing the total computational time. This is why we applied our fusion metamodel and the EGO optimization method described in Section 2 in two different scenarios.

In the first ‘‘calibrated’’ scenario, step 2 of the traditional three-step procedure was applied, i.e., the simulation model was pre-calibrated. In particular, for each investigated material with physical 3-point bending experiments available the  $K$  and  $n$  parameters ( $K$  and  $n$ ) of the three tested materials (Fe 360, Docol 800DP, AISI 304) were iteratively calibrated until the mismatch between experimental and numerical results felt below a 10% error threshold for the objective function  $y(48)$ . In other words, the FEM simulations were run again and again, changing  $K$  and  $n$ , until the error on  $y(48)$  was considered acceptable. Data used for the three initial materials in both scenarios are given in Table 2. As later shown in Section 4, 7 experimental design locations have been considered. In 1 out of 7 cases, no calibration was required, i.e. the error was already under 10%. In the other 6 locations, from 2 to 3 FEM runs were required in order to calibrate the input variable, for a total of about 15 additional computations. Please consider that calibrating the  $K$  and  $n$  values makes the  $x_1$  values change accordingly, i.e. the calibration has an effect on one of the two design variables. For additional materials, which have been evaluated only numerically, the tensile test hardening values found on the CES<sup>TM</sup> software package were used as a starting point for analytically calculating  $K$  and  $n$ .

In the second “non-calibrated” scenario, no time was spent for calibrating the simulation model, saving in this case the above mentioned 15 runs, each amounting to about 3 to 4 CPU hours with the workstation used in the study. All the materials, including the three materials with experimental values available, were simply modeled considering the nominal  $K$  and  $n$  values, calculated by the data given in CES<sup>TM</sup>.

By comparing the performance of the calibrated and non-calibrated scenarios we would like to demonstrate how the fusion metamodel can be used, to some extent, to reduce simulation calibration efforts.

	Non calibrated			Calibrated					
	All cross sections			Round cross section			Square section		
	$K$ [Mpa]	$n$	$x_1$ [Mpa]	$K$ [Mpa]	$n$	$x_1$ [Mpa]	$K$ [Mpa]	$n$	$x_1$ [Mpa]
Fe 360	603	0.20	73	603	0.20	73	530	0.26	77
DOCOL800DP	944	0.18	107	700	0.17	76	944	0.18	107
AISI 304	740	0.43	154	1133	0.43	235	-	-	-

**Table 2**  $K$  and  $n$  values for both scenarios

#### 4 Application of the method to the real case

The method described above has been applied to the crashworthiness optimization of aluminum foam filled tubular structures presented in 3. For both the calibrated and non-calibrated scenarios,  $n_h = 7$  experimental design locations were initially available. Every experimental combination, which is a tubular structure with its shape (summarized by  $x_2$ ) and outer material (summarized by  $x_1$ ) was replicated three times, for a total of  $n_h \times 3 = 21$  experimental (Hi-Fi) couples of  $y$  and  $x$  values. At these design locations, FEM simulations were performed for both the scenarios, i.e., with calibrated  $K$  and  $n$  values and with non-calibrated material data. Furthermore,  $n_l = 13$  additional design locations were added according to an initial random, space filling design of computer simulations (Lo-Fi data). A total of  $N_{des} = 20$  locations of  $y$  and  $x$  values were therefore originally available. The EGO algorithm embedded in the optimization routine suggested  $N_{ego} = 4$  additional evaluation points in the non-calibrated (Table 3) scenario and  $N_{ego} = 5$  in the calibrated one (Table 4). At each step of the EGO a metamodel and an optimization routine was built based on a minimum of  $N_{des} + N_{ego}$  design locations. Indeed, every new location suggested by the EGO approach, i.e. every new combination of  $x_1$  and  $x_2$  values, was “translated” into an actual material and an actual shape. Considering that it is not realistically possible to find an engineering material with exactly the  $x_1$  values suggested by the EGO, we considered the nearest available material option founded on the CES<sup>TM</sup> software package to be used instead. When more than one near option was found, all the close materials were tested. Similarly, it was difficult to define a real (i.e. potentially available on the market) tube cross section with the exact shape suggested by the EGO: the closest approximations was thus considered. For this reason, the actual number of

design locations tested was larger than  $N_{des} + N_{ego}$  for both scenarios: 27 instead of  $N_{des} + N_{ego} = 24$  locations were used in the non-calibrated scenario; 35 instead of  $N_{des} + N_{ego} = 25$  locations were used in the calibrated one.

Iteration	$x_1$	$x_2$
1	128.03	233.21
2	131.79	276.52
3	110.00	774.00
4	129.48	306.69

**Table 3** Evolution of the EGO algorithm in the non-calibrated scenario

Iteration	$x_1$	$x_2$
1	198.00	774.00
2	141.46	556.25
3	102.33	786.53
4	113.52	768.36
5	114.15	780.72

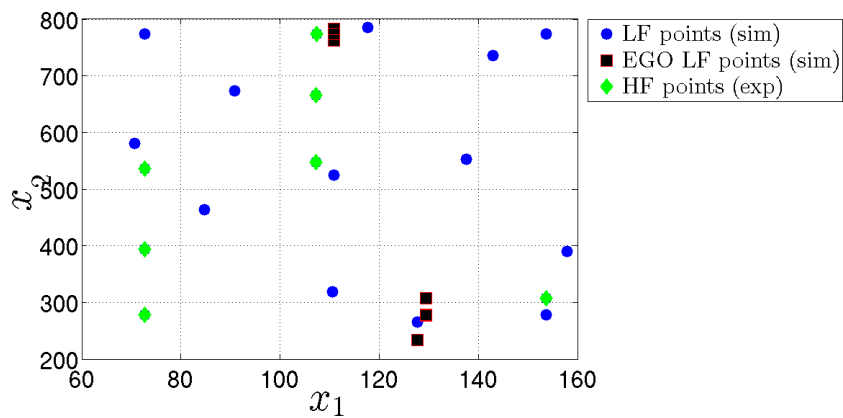
**Table 4** Evolution of the EGO algorithm in the calibrated scenario

It is useful to further clarify the differences between the two scenarios, with reference to Figure 8. In the design space, the variable  $x_1$  is a function of the material parameters under calibration,  $K$  and  $n$ . As a consequence, in the calibrated scenario, the experimental  $y$  values are placed in the design space at calibrated locations along the  $x_1$  axis. In the non-calibrated scenario, the experimental  $y$  values are still “reliable”, i.e. Hi-Fi, but they are located in the design space at non-calibrated  $x_1$  locations.

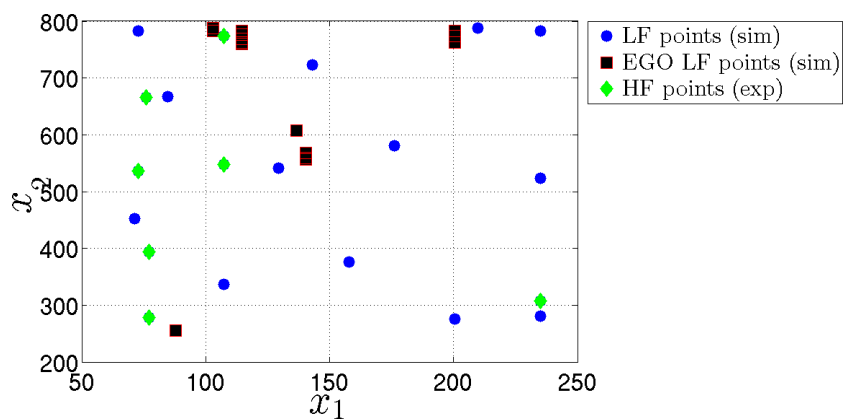
The optimal values of the non-calibrated and the calibrated scenario for each step of the EGO algorithm are reported in Table 5 and in Table 6, respectively. The resulting interpolated surface and the optimal solution for both the scenarios are shown in Figures 9 and 10, respectively. We observe that the values of the optimum found are not in an ascending order because during the steps of the algorithm there is also a re-estimation of the response function  $y$ .

Iteration	$x_1$	$x_2$	$y$
0	107.61	782.42	50 614.35
1	129.40	298.21	51 766.99
2	105.22	782.64	51 200.74
3	107.61	782.56	50 617.58
4	104.38	781.22	51 690.14

**Table 5** Evolution of the optimum during the EGO steps in the non-calibrated scenario



(a) Design space for non-calibrated scenario



(b) Design space for calibrated scenario

**Fig. 8** Design spaces

Iteration	$x_1$	$x_2$	$y$
0	107.05	777.39	50 376.07
1	107.16	770.56	50 130.40
2	107.12	776.63	50 376.73
3	113.52	785.20	49 129.89
4	113.15	786.77	52 490.92
5	114.57	774.76	52 712.46

**Table 6** Evolution of the optimum during the EGO steps in the calibrated scenario

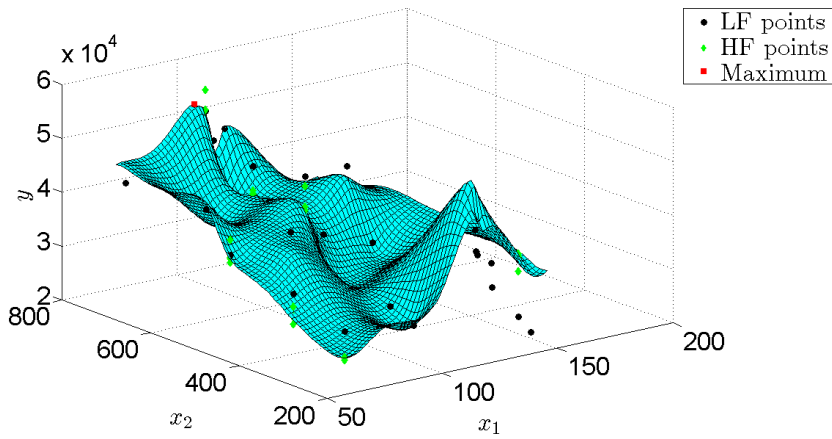


**Fig. 9** Surface of the metamodel for the non-calibrated scenario; optimal solution values are given in Table 5

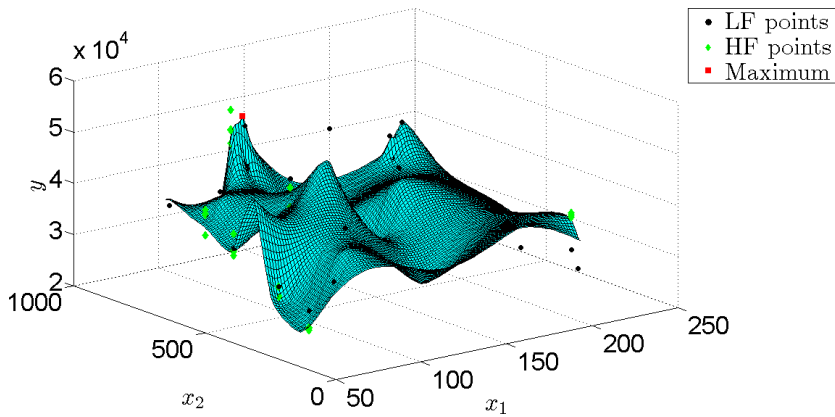


**Fig. 10** Surface of the metamodel for the calibrated scenario; optimal solution values are given in Table 6

By comparing the mentioned figures, we can observe how the two optimal  $\mathbf{x}$ -values are very similar, i.e. both scenarios yield more or less the same optimal solution. Furthermore, the estimated  $y(48)$  values are similar too, with a difference of only 0.1 %. The expected error of the optimal value of  $y(48)$  is smaller for the calibrated *vs.* the non-calibrated scenario (1764 *vs.* 5558  $\frac{N}{kg}$ ), which is not surprising, as the prediction yielded by the calibrated metamodel is obviously more accurate. Although the two scenarios yield the same optimal solution, the metamodeled surfaces are not very similar in shape. This is mainly because the calibration affects the  $x_1$  values and range.

#### 4.1 Further validation of the proposed approach

Looking at Figures 9 and 10, it is clear that several local maxima are present on the metamodeled surface. Some of these maxima, due to insufficient experimental data, might be erroneously evaluated by the models built respectively with calibrated and non-calibrated data. In order to assess whether the optimal solution found is a true optimum, additional experiments were planned and executed with two more tube materials (Docol 600 DP and AISI 316L). These additional points also serve for validating the accuracy of the prediction offered by both the metamodels. Both the tubes are round shaped. Their geometrical data, the calibrated material properties and the corresponding  $x_1$  and  $x_2$  values are given in Table 7. If these two Hi-Fi points are added to the metamodel in Figure 10, the surface changes as shown in Figure 11, but the optimal solution is virtually unaltered. Similar results were obtained by repeating the procedure in the non-calibrated scenario.

	$K$ [MPa]	$n$	$x_1$ [MPa]	$x_2$ [mm <sup>3</sup> ]
DOCOL800DP	903	0.15	87.90	254.80
AISI 316L	965	0.25	136.70	607.30

**Table 7**  $K$ ,  $n$  values and  $\mathbf{x}$  values to be added to the calibrated scenario

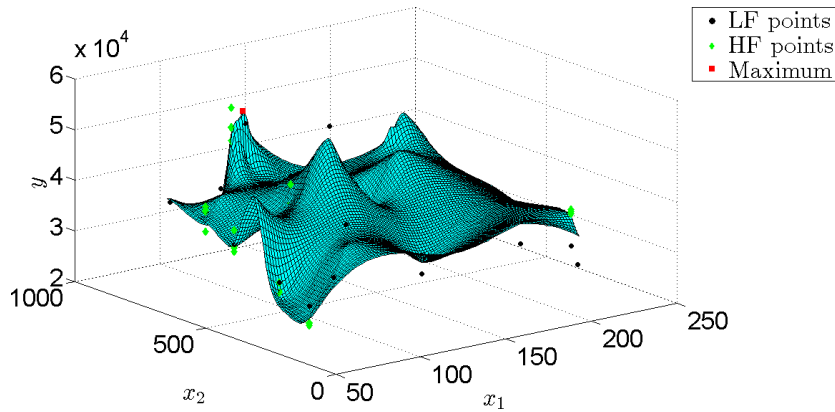


**Fig. 11** Surface of the metamodel for the calibrated scenario with two more Hi-Fi points added

In order to test the credibility of both the metamodels, we made a “leave-one-out” cross validation at the three closest available Hi-Fi locations to the calculated output, the results of the square root of the MSE are in Table 8. “Leave-one-out” means that the metamodel is rebuilt every time using only the Hi-Fi points from 6 locations, not 7 as in the full plan. This additional study clearly proves that both metamodels closely predict the real values in the region where the optimum is finally found because the square root of the MSE is small compared to the

ranges of the three variables (in the order of 100, 780 and 52 000 for  $x_1$ ,  $x_2$  and  $y$ , respectively). In other words, the optimum found is the same for both models and can be considered a credible solution.

Scenario	RMSE( $x_1$ )	RMSE( $x_2$ )	RMSE( $y$ )
Non calibrated	1.50	28.38	576.46
Calibrated	0.76	13.64	183.96

**Table 8** Square root of the MSE of variable  $x_1$ ,  $x_2$ , and  $y$ .

Finally, in order to verify the accuracy of both the metamodels, the prediction yielded by the reconstructed surfaces in Figures 9 and 10 was compared with the Hi-Fi values obtained. The prediction errors are given in Table 9, which clearly shows how both the models can be considered similar in terms of their predicting ability.

	Non calibrated		Calibrated	
	Predicted $y(48)$	% Error on the experimental Hi-Fi value	Predicted $y(48)$	% Error on the experimental Hi-Fi value
DOCOL800DP	28 315.81	4.09 %	26 941.87	8.74 %
AISI 304	39 888.42	8.52 %	39 656.30	9.05 %

**Table 9**  $K$  and  $n$  values for both scenarios

## 5 Conclusions

In this paper, a metamodeling optimization method was proposed, based on a hierarchical “fusion” combination of both experimental (Hi-Fi) and numerical (Lo-Fi) data. The model was applied to the structural optimization of an aluminum foam filled steel tube, aimed at the absorption of mechanical energy as a side bar in vehicles. Experimental three point bending tests were performed with different tube shapes and materials and two designed plans of numerical simulations were implemented, too, according to two scenarios. In the first scenario, the simulation hardening data for the experimentally tested tubular materials were calibrated until the prediction error was below 10%. In the second scenario no calibration was performed and nominal values were used for modeling the flow stress of steel cases. The study showed how the optimization algorithm, run with both the scenarios, yield the same optimum solution and how both the models have a similar predicting ability. In the proposed example, the “fusion” metamodeling approach worked as an effective tool in order to reduce the time and effort spent in calibration of input simulation data.

## References

- Baghdasaryan L, Chen W, Buranathiti T, Cao J (2002) Model validation via uncertainty propagation using response surface models. In: Detc2002/dac-34140, pp 1–12
- Do T, Fourment L, Laroussi M (2004) Sensitivity analysis and optimization algorithms for 3d forging process design. In: AIP Conference Proceedings 712, p 20262031
- Friedman L, Pressman I (1988) The metamodel in simulation analysis: Can it be trusted? *The Journal of the Operational Research Society* 39(10):939–948
- Harville D (1977) Maximum likelihood approaches to variance component estimation and to related problems. *Journal of the American Statistical Association* 72:320–338
- Hino R, Yoshida F, Toropov V (2006) Optimum blank design for sheet metal forming based on the interaction of high- and low-fidelity fe models. *Archive of Applied Mechanics* 75:679–691
- Huang D, Allen T, Notz W, Miller R (2006a) Sequential kriging optimization using multiple-fidelity evaluations. *Structural and Multidisciplinary Optimization* 32(5):369–382
- Huang D, Allen T, Notz W, Zheng N (2006b) Global optimization of stochastic black-box systems via sequential kriging meta-models. *Journal of Global Optimization* 34:441–466
- Jones D, Schonlau D, Matthias Welch W (1998) Efficient global optimization of expensive black-box functions. *Journal of Global optimization* 13:455–492
- Kennedy M, O’Hagan A (2000) Predicting the output from a complex computer code when fast approximations are available. *Biometrika* 87:1–13
- Mockus J, Tiesis V, Zilinskas A (1978) The application of bayesian methods for seeking the extremum. In: *Towards Global Optimization*
- Pagani L (2011) Multisensor data fusion for quality inspection of free-form surfaces. Master’s thesis, Politecnico di Milano
- Qian Z, Seepersad C, Joseph V, Allen J, Wu C (2006) Building surrogate models based on detailed and approximate simulations. *ASME Journal of Mechanical Design* 128:668–677
- Roux E, Bouchard P (2013) Kriging metamodel global optimization of clinching joining processes accounting for ductile damage. *Journal of Materials Processing Technology* 213:10,387–1047
- Santner T, Williams B, Notz W (2003) *The Design and Analysis of Computer Experiments*. Springer Verlag
- Shabenberger O, Gotway C (2005) *Statistical Methods for Spatial Data Analysis*. Chapman & Hall/CRC
- Strano M, Mussi V, Monno M (2010) Non-conventional technologies for the manufacturing of anti-intrusion bars. *International Journal of Material Forming* 3:1111–1114
- Sun G, Li G, Zhou S, Xu W, Yang X, Li Q (2010) Multi-fidelity optimization for sheet metal forming process. *Structural and Multidisciplinary Optimization* 44(1):111–124
- Wagner T, Bröcker C, Saba N, Biermann D, Matzenmiller A, Steinhoff K (2011) Modelling of a thermomechanically coupled forming process based on functional outputs from a finite element analysis and from experimental measurements.

- AStA *Advances in Statistical Analysis* 94(4):389–404
- Wiebenga H, Boogaard A, Klaseboer G (2012) Sequential robust optimization of a v bending process using numerical simulations. *Structural and Multidisciplinary Optimization* 46:137–156
- Xia H, Yu Din Y, Mallick B (2011) Bayesian hierarchical model for combining misaligned two resolution metrology data. *IIE Transactions* 43:242–258
- Yu B, Popplewell K (1994) Metamodels in manufacturing: a review. *International Journal of Production Research* 32(4):787–796
- Yuen S, Nurick G (2008) The energy-absorbing characteristics of tubular structures with geometric and material modifications: An overview. *Transactions of the ASME: Applied Mechanics Reviews* 61:1–15
- Zarei H, Kroger M (2008) Bending behavior of empty and foam-filled beams: Structural optimization. *International Journal of Impact Engineering* 35:521–529
- Zsolt U, Lasdon L, Plummer J, Glover F, Kelly J, Martí R (2007) Scatter search and local nlp solvers: A multistart framework for global optimization. *Journal on Computing* 19:328–340